frontiers | Frontiers in Energy Research

ORIGINAL RESEARCH
published: 09 May 2022
doi: 10.3389/fenrg.2022.882508

Moisture Stability of Sulfide Solid-State Electrolytes

Thomas A. Yersak[1], Yubin Zhang[2], Fang Hao[2] and Mei Cai[1]*

[1]*Battery Cell Systems Research Laboratory, General Motors Global R&D, Warren, MI, United States,* [2]*Optimal, Inc., Plymouth, MI, United States*

In this report we detail a comprehensive study on the moisture stability of sulfide solid-state electrolytes in dry room environments. Although sulfide SSEs have many favorable attributes, this class of materials suffers from poor stability with water. Sulfide SSEs react with water to form gaseous H_2S and a variety of solid byproducts like Li_3PO_4 and LiOH, which go on to increase the interfacial impedance of solid-state batteries. Lab-scale research typically utilizes gloveboxes with <1 ppm water, however, the large-scale manufacturing of Li-ion batteries occurs in −40°C dewpoint dry rooms with around 126 ppm water. Consequently, the moisture stability of sulfide SSEs must be addressed if the manufacture of solid-state batteries based on sulfide SSEs is to be scaled up. Here, we are the first to characterize the moisture stability of sulfide SSEs according to both H_2S and the degradation of ionic conductivity at different moisture setpoints ranging from −76°C to −40°C dewpoint. A variety of different SSE compositions are studied; namely, $(Li_2S)_{75}(P_2S_5)_{25}$, $(Li_2S)_{70}(P_2S_5)_{30}$, $(Li_2O)_7(Li_2S)_{68}(P_2S_5)_{25}$, $(Li_2O)_7(Li_2S)_{63}(P_2S_5)_{30}$, and $(Li_2S)_{75}(P_2S_5)_{25}$ + 20 mol% LiI. We find that moisture stability improves with 75 mol% Li_2S modifier content and the introduction of a Li_2O co-modifier. After a 30 min exposure in a −40°C dewpoint dry room environment we found that $(Li_2S)_{75}(P_2S_5)_{25}$ + 20 mol% LiI powder generated 0.1 cc/g H_2S and its ionic conductivity decreased by over 50%. However, when SSE powder was exposed as a slurry in a dodecane carrier the same SSE composition generated 0 cc/g H_2S and its ionic conductivity only dropped by 14%. Our results show that sulfide SSEs have acceptable moisture stability when appropriately processed in a dry room environment.

Keywords: sulfide, solid-state, moisture stability, ionic conductivity, dry room

OPEN ACCESS

Edited by:
Hui Wang,
University of Louisville, United States

Reviewed by:
Yang Zhao,
Western University, Canada
Jun Zhang,
Zhejiang University of Technology, China

****Correspondence:***
Thomas A. Yersak
thomas.yersak@gm.com

Specialty section:
This article was submitted to Electrochemical Energy Conversion and Storage, a section of the journal Frontiers in Energy Research

Received: *23 February 2022*
Accepted: *06 April 2022*
Published: *09 May 2022*

Citation:
Yersak TA, Zhang Y, Hao F and Cai M (2022) Moisture Stability of Sulfide Solid-State Electrolytes. Front. Energy Res. 10:882508. doi: 10.3389/fenrg.2022.882508

INTRODUCTION

Sulfide solid-state electrolytes (SSEs) have garnered much interest in academia and industry due to their high ionic conductivity up to 10^{-2} S/cm and good processability (Zhang et al., 2020; Zheng et al., 2021a; Chen et al., 2021; Pang et al., 2022). Unfortunately, the poor moisture stability of sulfide SSEs presents a major obstacle to the commercialization of solid-state batteries utilizing these SSEs (Hao et al., 2018; Chen et al., 2019; Randau et al., 2020). In academic studies, sulfide SSEs are typically handled in inert gloveboxes with a moisture content of <1 ppm H_2O (−80°C dew point) since they are readily hydrolyzed by moisture in air to release H_2S. For context, conventional Li-ion batteries are typically assembled in dry rooms with −40°C dew point (127 ppm H_2O). If sulfide SSE-based solid-state batteries are to be manufactured using the same capital equipment and facilities as those used to make conventional Li-ion batteries, then the moisture stability of sulfide SSEs must be improved.

Accordingly, previous studies have evaluated the moisture stability of $xLi_2S{\cdot}(100\text{-}x)P_2S_5$ sulfide SSEs with different compositions (Muramatsu et al., 2011), with additives (Ohtomo et al., 2013a; Hayashi et al., 2013; Hayashi et al., 2014), with a Li_2O co-modifier (Ohtomo et al., 2013b; Ohtomo et al., 2013c; Ohtomo et al., 2013d), with a LiI dopant (Calpa et al., 2021), or with a hydrophilic binder (Tan et al., 2019).

The aforementioned studies used H_2S generation as a proxy for moisture stability. H_2S generation is an important metric from a safety perspective (Evans, 1967), however, no data has been published on how well sulfide SSEs retain their ionic conductivity after exposure to air. Furthermore, previous work evaluated the moisture stability of sulfide SSEs under ambient conditions and often moisture level was not reported. If ambient condition is considered to be air at a temperature of 25°C and 30% relative humidity, then this equates to an extremely high water content of 0.95% by volume (9,500 ppm). It is much better to characterize the moisture stability of sulfide SSEs under conditions that match those of a cell manufacturing plant. In this study, we therefore report the moisture stability of sulfide SSEs in a dry room environment and quantify moisture stability as both H_2S generation and how well a sulfide SSE retains its ionic conductivity after exposure.

We will first present the stability of several glass sulfide SSE compositions when exposed in a −40°C dew point dry room to obtain a comprehensive understanding for how sulfide glass composition influences hygroscopicity. Sulfide SSEs compositions were chosen to probe the influence of glass modifier (Li_2S) content, glass co-modifier (Li_2O), and LiI dopant. A description of these glass SSE constituents can be found elsewhere (Martin, 2016). The five different SSE compositions studied were $(Li_2S)_{75}(P_2S_5)_{25}$, $(Li_2S)_{70}(P_2S_5)_{30}$, $(Li_2O)_7(Li_2S)_{68}(P_2S_5)_{25}$, $(Li_2O)_7(Li_2S)_{63}(P_2S_5)_{30}$, and $(Li_2S)_{75}(P_2S_5)_{25}$ + 20 mol% LiI. Consistent with previous studies, we generally found that glasses with 75 mol% of modifier content yielded the best moisture stability (Muramatsu et al., 2011). Raman spectroscopic analysis of samples before and after exposure determined that the comparatively stable PS_4^{3-} structural unit accounts for the moisture stability of these samples. Our results also show that the $(Li_2O)_7(Li_2S)_{68}(P_2S_5)_{25}$ SSE produced nearly zero H_2S after a 30 min exposure to a −40°C dew point dry room, but its ionic conductivity still dropped by over 50%. We conclude that any quantification of moisture stability must therefore consider the ionic conductivity of the sulfide SSE after exposure. Our study then evaluated the moisture stability of the $(Li_2S)_{75}(P_2S_5)_{25}$ + 20 mol% LiI SSE as a function of dry room moisture level from −40 to −76°C dew point. Degradation of sulfide SSE ionic conductivity was found to be nonlinear with respect to H_2O concentration. As a final test, the moisture stability of sulfide SSE slurries was evaluated to mimic the handling of SSE material during an electrode or separator tape casting process (Zheng et al., 2021b). The $(Li_2S)_{75}(P_2S_5)_{25}$ + 20 mol% LiI SSE was suspended in either anhydrous dodecane or anisole and exposed to a dry room environment with −40°C dew point. The dodecane slurry generated zero H_2S and the sulfide SSE retained 95.3% of its pristine ionic conductivity. The results of this study suggest that even though sulfide SSEs are hygroscopic, there are ways to handle sulfide SSEs in a typical cell manufacturing environment without damaging the sulfide SSEs' function.

MATERIALS AND METHODS

During preparation all materials were handled under an argon atmosphere with less than 1 ppm water and oxygen. Solid-state electrolyte (SSE) precursor materials included Li_2S (99.5% Sigma Aldrich), Li_2O (99.5%, Alfa Aesar), P_2S_5 (98% Sigma Aldrich), and LiI (99.9%, Aldrich). Five different SSE compositions were prepared: $(Li_2S)_{75}(P_2S_5)_{25}$ (75-25 LPS), $(Li_2S)_{70}(P_2S_5)_{30}$ (70-30

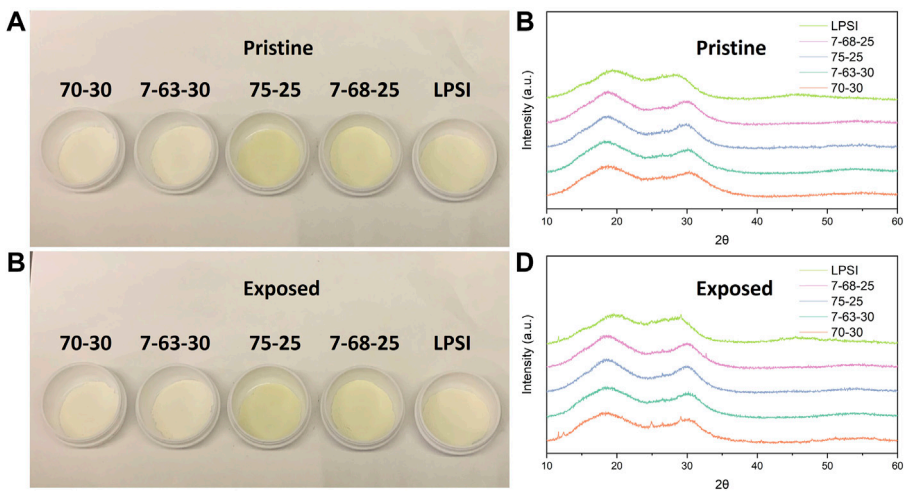

FIGURE 1 | (A) A picture of the pristine sulfide SSE powders. **(B)** Powder XRD patterns of the pristine glassy SSEs. **(C)** A picture of the sulfide SSE powders after exposed in dry room. **(D)** Powder XRD patterns of the glassy SSEs. after exposed in dry room.

FIGURE 2 | A picture of the experimental setup used to expose sulfide SSE powders to a dry room environment. The setup includes a 300L volume tabletop glovebox, a cartridge-based desiccant system, a microcontroller system to control the moisture setpoint, a personal H_2S detector, and a fan to continuously mix the glovebox air.

LPS), $(Li_2O)_7(Li_2S)_{68}(P_2S_5)_{25}$ (7-68-25 LPSO), $(Li_2O)_7(Li_2S)_{63}(P_2S_5)_{30}$ (7-63-30 LPSO), and $(Li_2S)_{75}(P_2S_5)_{25}$ + 20 mol% LiI (LPSI). SSEs were prepared by planetary ball milling (Frisch Pulverisette 7). In this process, 4g SSE precursors of the appropriate stoichiometry were first combined in a 40 ml zirconia milling jar along with 10 ml of dried hexane (4Å molecular sieve) and 80 g of milling media. Next, each sample was milled for total of 20 h at 500 rpm. Finally, the hexane was removed by gently heating opened milling jars at 60°C for 12 h. SSE powders were pale yellow to off-white in color as shown in **Figure 1A**.

The long-range structure of glasses was studied using powder x-ray diffraction (pXRD) (Bruker D8 Advance). pXRD data are provided in **Figure 1B**, and the absence of strong reflections indicate that all samples are amorphous. A weak reflection at approximately 27° 2θ indicates some samples do have trace amounts of Li_2S (Jain et al., 2013). The implications of trace Li_2S on moisture stability will be discussed in the next section. The short-range structure of glasses before and after exposure to a dry room environment was studied using Raman spectroscopy (Renishaw InVia) with a 532 nm excitation line and a ×20 objective lens.

An actual dry room was not used in this study. Rather, a dry room environment was simulated inside a 300 L tabletop acrylic glovebox (MBraun, MB-GB-2202) using synthetic air (Airgas, AI UZ300, 76.5–80.5% nitrogen, 19.5–23.5% oxygen) as shown in **Figure 2**. The glovebox was outfitted with a custom moisture control system to maintain humidity levels to within ±2°C of a desired target dew point. Unless otherwise noted, the humidity level was set to −40°C dew point (127 ppm H_2O) for each experiment. The control system consisted of a cartridge-based desiccator (VAC, Genesis), a moisture probe (VAC, LM-H_2O-A), and an Arduino microcontroller. The microcontroller was programmed to monitor the moisture probe voltage output and send a digital signal to a solid-state relay that turned the desiccator fan on and off as needed. The desiccant system was disabled during SSE exposure experiments since it also scrubbed H_2S from the atmosphere. During each experiment, 0.6 g of sulfide SSE powder was spread out onto a flat surface and exposed to air for 30 min. The exposure of powder more closely mimics an actual manufacturing process than the exposure of compacted pellets. A fan was run to constantly mix the atmosphere within the glovebox to ensure a uniform mix of H_2O and H_2S. H_2S concentration was measured using a personal safety sensor (ToxiRAE) oriented 4 inches above the sample powder as shown in **Figure 2**. After exposure, the SSE powder was packaged in a glass vial and transferred back into an argon atmosphere with less 1 ppm water and oxygen. The box was cleaned and purged between each experiment to ensure a 0.0 ppm H_2S starting baseline. Scanning electron microscopy (SEM) (Hitachi S-4800) was used to observe the morphology before and after exposure. Energy-dispersive X-ray spectroscopy (EDS) (Ametek EDAX) equipped on the SEM was used to characterize the SSE elemental compositions before and after exposure.

The ionic conductivity of sulfide SSEs was measured by assembling Li/SSE/Li symmetric cells with SSE powder

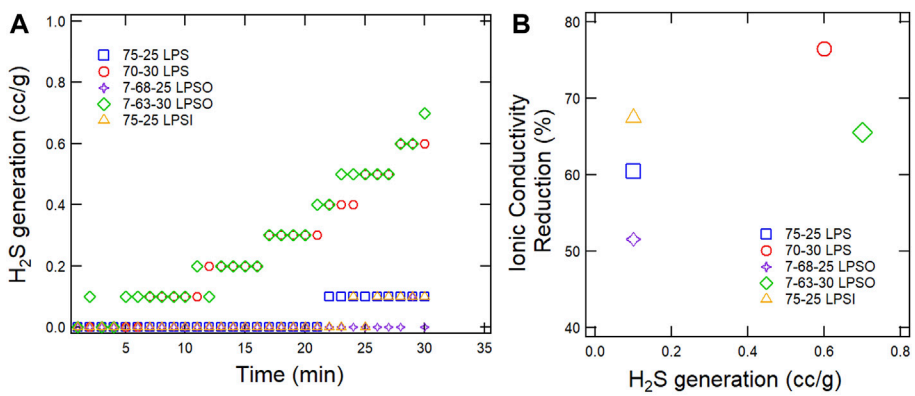

FIGURE 3 | (A) H_2S generation of different SSEs in a −40°C dew point dry room as a function of time. **(B)** Reduction in ionic conductivity versus maximum H_2S reading for different sulfide SSEs.

TABLE 1 | Ionic conductivity and H2S generation data for sulfide SSE powders exposed to a –40°C dew point dry room environment for 30 min.

Composition	Pristine σ (mS/cm)	Exposed σ (mS/cm)	Δσ	H_2S generation (cc/g)
$(Li_2S)_{75}(P_2S_5)_{25}$	0.43	0.17	–60.5%	0.2
$(Li_2O)_7(Li_2S)_{68}(P_2S_5)_{25}$	0.31	0.15	–51.6%	0.1
$(Li_2S)_{70}(P_2S_5)_{30}$	0.26	0.061	–76.5%	0.6
$(Li_2O)_7(Li_2S)_{63}(P_2S_5)_{30}$	0.18	0.062	–65.6%	0.7
$(Li_2S)_{75}(P_2S_5)_{25}$ + 20 mol% LiI	1.21	0.39	–67.8%	0.1

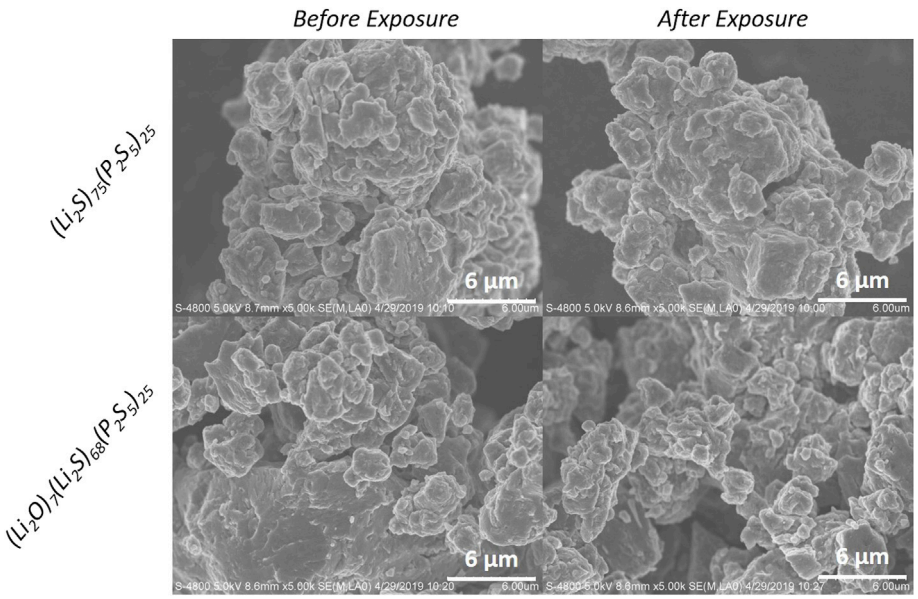

FIGURE 4 | SEM images of 75-25 LPS and 7-68-25 LPSO sulfide SSEs before and after exposure.

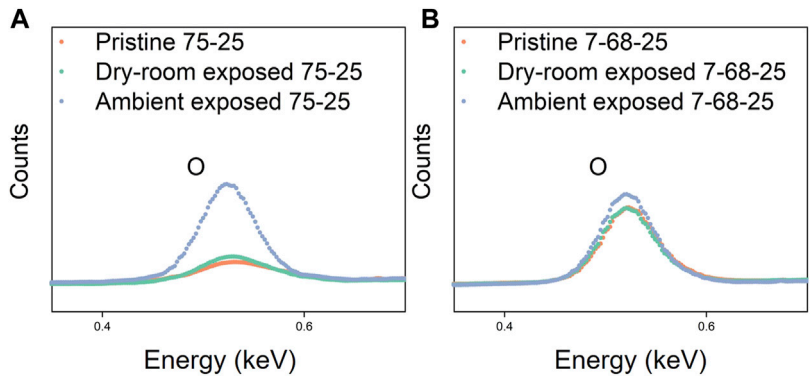

FIGURE 5 | EDS oxygen Kα principle line (0.52 keV) for 75-25 LPS **(A)** and 7-68-25 LPSO **(B)** before (red) and after exposure to either a dry room environment (green) or ambient air (blue).

collected before and after exposure to air. To assemble each cell, 150–200 mg of sulfide SSE powder was compacted using a 13 mm diameter polyetheretherketone (PEEK) die and stainless steel plungers with a pressure of 370 MPa. Li metal foil (MTI, 0.5 mm thick) was then attached to both sides of the compacted SSE powder disc. AC impedance of these cells was then measured immediately after assembly using a frequency range 1 MHz to 0.1 Hz and an excitation current of 10 µA

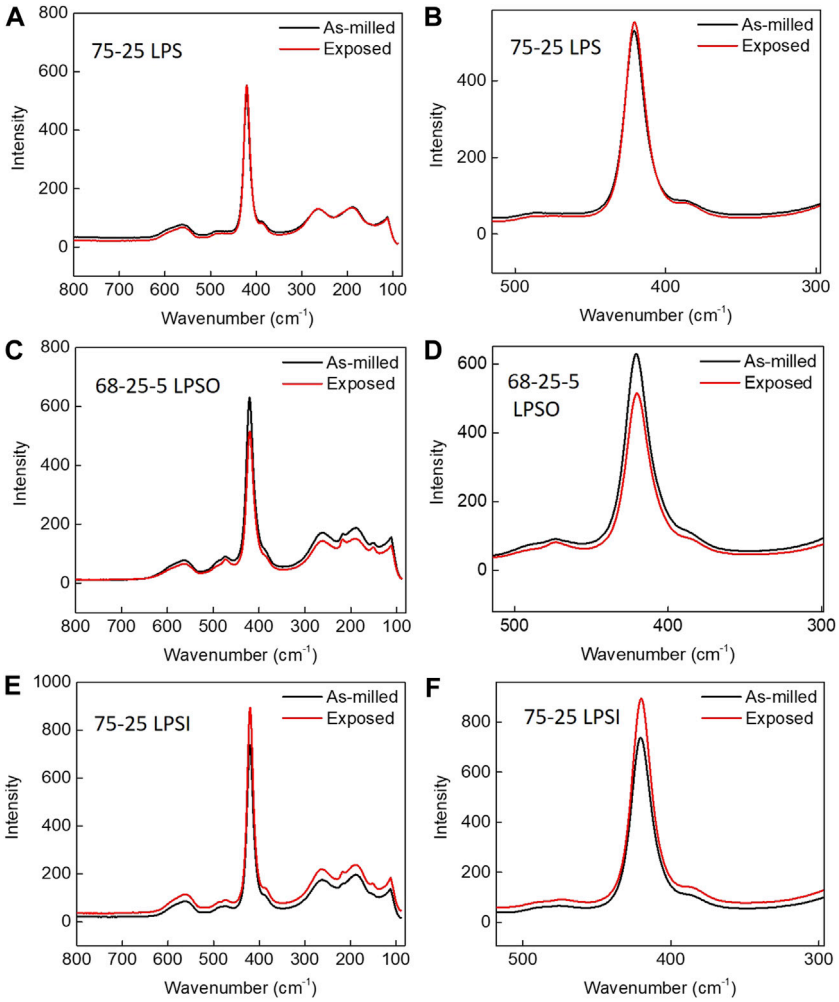

FIGURE 6 | Raman spectroscopy spectra for 75-25 LPS, 7-68-25 LSPO, and LPSI sulfide SSEs before and after exposure to a –40°C dew point dry room for 30 min.

(Biologic VMP-3). Total real impedances (R_T) were interpolated from the minima of the Nyquist plot spectra. The thickness (t) and area (a) of each glass sample was measured using digital calipers and ionic conductivity was then calculated using **Eq. 1** from values of R_T, t and a.

$$\sigma = \frac{t}{aR_T} \tag{1}$$

RESULTS AND DISCUSSION

In the first experiment of this study, a variety of sulfide SSE powders were exposed to a −40°C dew point dry room environment for 30 min. During this experiment H_2S gas generation was monitored and the data are provided in **Figure 3A**. Our results are consistent with the findings of previous studies with respect to the influence of glass modifier (Li_2S) content, glass co-modifier (Li_2O), and LiI dopant on H_2S generation. First, sulfide SSEs with 75 mol% glass modifier produced the least amount of H_2S (Muramatsu et al., 2014). 75-25 LPS, 7-68-25 LPSO, and 75-25 LPSI all generated a maximum of 0.1 g/cc H_2S, whereas 70-30 LPS and 7-63-30 LPSO generated a maximum of 0.6–0.7 g/cc H_2S. Second, a Li_2O co-modifier modestly reduced the H_2S generation of sulfide SSEs (Ohtomo et al., 2013b; Ohtomo et al., 2013c; Ohtomo et al., 2013d). Even though our H_2S device had a resolution of only 0.1 ppm, which is equivalent to 0.1 cc/g, we could still track the time it took before each sample registered a non-zero value. 75-25 LPS registered its first non-zero value at 22 min whereas 7-68-25 LPSO only registered one non-zero value at 29 min. No appreciable difference was observed between 70 and 30 LPS and 7-63-30 LPSO. Finally, a LiI dopant did not increase H_2S generation since both 75-25 and 75-25 LPSI generated a maximum of 0.1 g/cc H_2S (Ohtomo et al., 2013c). Calpa et al. (2021) previously reported that a LiI dopant reduces the H_2S generation of sulfide SSEs exposed to ambient air at 40% relative humidity. Our study differed from Calpa et al. in that our

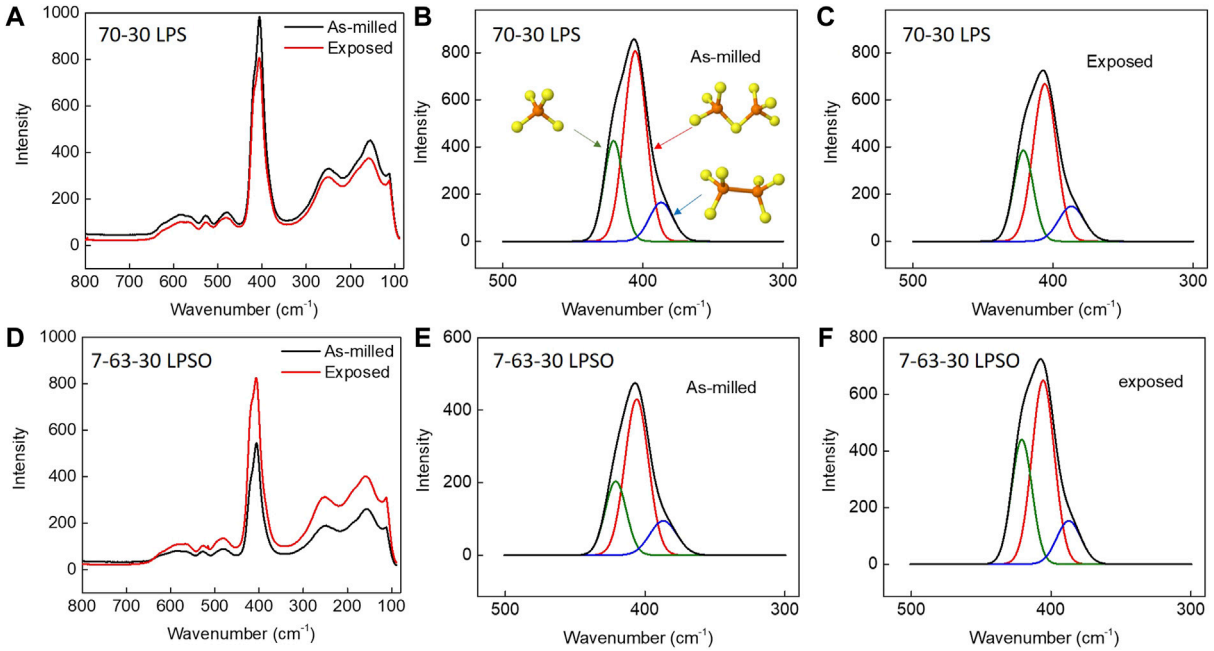

FIGURE 7 | Raman spectra of sulfide SSEs before and after exposure to a −40°C dew point dry room environment for 30 min. The primary peak was deconvoluted into three peaks attributed to PS_4^{3-} (green, 420 cm−1), $P_2S_7^{4-}$ (red, 406 cm−1), and $P_2S_6^{4-}$ (blue, 387 cm−1) structural units. **(A)** Raman spectra for 70-30 LPS before and after exposure. **(B)** Fitted Raman spectrum for 70-30 LPS before exposure. Insets provide ball and stick models for PS_4^{3-}, $P_2S_7^{4-}$, and $P_2S_6^{4-}$ structural units. **(C)** Fitted Raman spectrum for 70-30 LPS after exposure. **(D)** Raman spectra for 7-63-30 LPSO before and after exposure. **(E)** Fitted Raman spectrum for 7-68-30 LPSO before exposure. **(F)** Fitted Raman spectrum for 7-68-30 LPSO after exposure.

TABLE 2 | Summary of Raman spectra peak fitting and deconvolution.

Sample	PS_4^{3-} (%)(421 cm^{-1})	$P_2S_7^{4-}$ (%) (406 cm^{-1})	$P_2S_6^{4-}$ (%) (387 cm^{-1})
Pristine $(Li_2S)_{70}(P_2S_5)_{30}$	27.0	60.2	12.8
Exposed $(Li_2S)_{70}(P_2S_5)_{30}$	28.2	57.8	14.0
Pristine $(Li_2O)_7(Li_2S)_{63}(P_2S_5)_{30}$	25.3	59.7	15.0
Exposed $(Li_2O)_7(Li_2S)_{63}(P_2S_5)_{30}$	33.1	53.3	13.6

moisture level was much lower and we exposed SSE powder instead of pellets.

In addition to monitoring H_2S gas generation, this study is the first to report on the ionic conductivity of sulfide SSEs before and after exposure to a −40°C dew point dry room environment and the data are provided in **Figure 3B** and **Table 1**. Every sample experienced a significant drop in ionic conductivity with 70-30 LPS having the largest drop of 76.5% and 7-68-25 LPSO having the smallest drop of 51.6%. The products of sulfide SSE hydrolysis may include compounds such as LiOH (Muramatsu et al., 2014), Li_3PO_4 (Ohtomo et al., 2013a), and $LiI{\cdot}H_2O$ (Calpa et al., 2021). These compounds are poor ionic conductors, and if formed on the surface of sulfide SSE particles will act to substantially increase interparticle impedance once the powders are consolidated into pellets or films. We conclude that H_2S generation is not a sufficient metric for the moisture stability of sulfide SSEs and that moisture stability should also comprehend functional characteristics like ionic conductivity.

In the next phase of this work the SSEs were characterized with pXRD, SEM, Raman spectroscopy, and EDS to understand the effect of hydrolysis on SSE particle morphology and SSE structure. After exposure the SSE powders appeared unchanged (**Figure 1C**) and no new reflections were detected by pXRD (**Figure 1D**). The pXRD data suggest that the products of SSE hydrolysis in a dry room environment were either amorphous or in a small quantity below the detection limit of our equipment. SEM images of 75-25 LPS and 7-68-25 LPSO before and after exposure are provided in **Figure 4**. SSE particles range in size from approximately 1 μm to greater than 10 μm in diameter and no discernable difference was observed after exposure. Finally, the elemental compositions of the 75-25 LPS and 7-68-25 LPSO were characterized using EDS. **Figure 5** provides the EDS oxygen Kα principle line (0.52 keV) for SSEs before and after exposure. All EDS spectra were normalized to the phosphorus Kα principle line (2.01 keV) and the full dataset is provided in **Supplementary Figure S1**. The pristine samples both

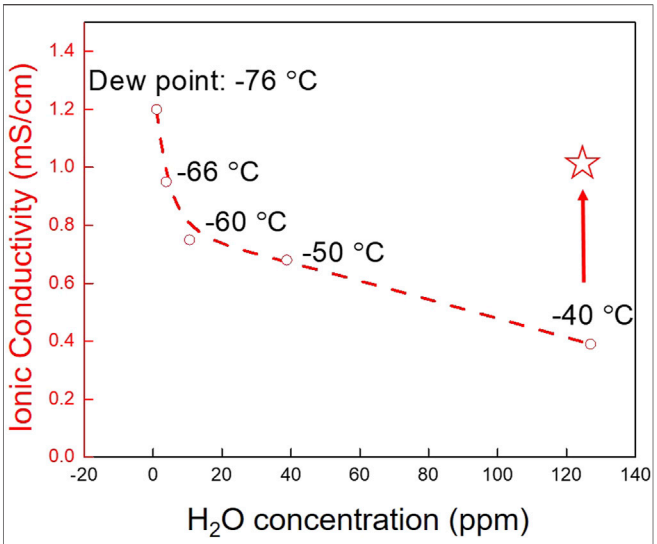

FIGURE 8 | Ionic conductivity of LPSI sulfide SSE after exposure as a dry powder to different dry room environments for 30 min. The star marks the ionic conductivity of LPSI sulfide SSE after exposure to a −40°C dew point dry room for 30 min while immersed in anhydrous dodecane.

exhibit an oxygen signal (red). An oxygen signal is expected for 7-68-25 LPSO since it contains a Li_2O co-modifier. The oxygen signal for 75-25 LPS can be explained by precursor impurities and a brief exposure to ambient air during sample transfer to the SEM. After dry room exposure (−40°C dewpoint) for 30 min the oxygen signal for 75-25 LPS increased slightly while that of the 7-68-25 LPSO remained unchanged (green). To effect a measurable change on both samples we also exposed SSEs to ambient air (20°C, 20% relative humidity) for 5 min. In this case, both samples exhibit a substantially increased oxygen signal (blue). As we will discuss later on, an increase in the oxygen signal suggests that the hydrolysis of SSEs leads to the formation of oxygen containing compounds.

The local structure of sulfide SSEs before and after exposure was determined by Raman spectroscopy and the data are provided in **Figure 6**, **Figure 7**, and **Table 2**. **Figure 6** presents the Raman spectra for sulfide SSEs with 75 mol% modifier content; namely, 75-25 LPS, 7-68-25 LPSO, and 75-25 LPSI. The spectra for these sulfide SSEs are dominated by a single feature centered at 421 cm^{-1} attributable to the PS_4^{3-} structural unit. After exposure, this feature does not shift or change shape suggesting that the local structure of sulfide SSEs with 75 mol% modifier content remains the same. **Figure 7** presents the Raman spectra for sulfide SSEs with 70 mol% modifier content; namely, 70-30 LPS and 7-63-30 LPSO. Similarly, the spectra are dominated by a single feature, however, this feature may be deconvoluted into multiple peaks attributable to PS_4^{3-} (421 cm^{-1}), $P_2S_7^{4-}$ (406 cm^{-1}), and $P_2S_6^{4-}$ (387 cm^{-1}) structural units (**Figures 7B,E**; **Table 2**).The local structure of sulfide SSEs with 70 mol% modifier content is more complicated since the glass former is not fully de-networked. This results in the formation of larger structural units like $P_2S_7^{4-}$ and $P_2S_6^{4-}$, which are more susceptible to hydrolysis due to labile bridging sulfur and P-P bonds, respectively (Tan et al., 2019). In fact, after exposure the relative abundance of $P_2S_7^{4-}$ and $P_2S_6^{4-}$ structural units decreased compared to that of PS_4^{3-} (**Figures 7C,F**; **Table 2**). For example, the peak area attributable to PS_4^{3-} went from 25.3% before exposure to 33.1% after exposure for 7-63-30 LPSO (**Table 2**). From these data we conclude that the PS_4^{3-} structural unit is comparatively more stable than $P_2S_7^{4-}$ or $P_2S_6^{4-}$. Sulfide SSEs with 75 mol% modifier content therefore produce less H_2S because they are primarily composed of PS_4^{3-} structural units, which react with moisture at a slower rate than the larger structural units found in sulfide SSEs with 70 mol% modifier content.

We just outlined the mechanism for how modifier content affects moisture stability. Before moving on to the results of the last two experiments, let's first consider the effect that a Li_2O co-modifier or LiI dopant may have on ionic conductivity. Both Li_2O and LiI were found to reduce the generation of H_2S; however, we just showed that ionic conductivity was significantly degraded irrespective of sulfide SSE composition (**Table 1**). It was previously suggested that Li_2O may displace excess, unreacted Li_2S and that unreacted Li_2S is a significant source of H_2S gas (Ohtomo et al., 2013b; Muramatsu et al., 2014). In fact, several of our samples do have a trace amount of Li_2S as evidenced by a weak reflection at about 27° 2θ in pXRD data of pristine samples (**Figure 1B**). Li_2S reacts with H_2O to form LiOH and H_2S gas as shown in **Eq. 2**. Li_2O also reacts with H_2O to form LiOH, but it does not release H_2S gas as shown in **Eq. 3**. Similarly, LiI reacts with H_2O to form LiI·H_2O as shown in **Eq. 4**. These reaction schemes are supported by the aforementioned EDS data, which show a higher prevalence of oxygen in SSE samples after exposure to air (**Figure 5**; **Supplementary Figure S1**). As stated earlier, H_2S generation is an insufficient measure of moisture stability. Both Li_2O and LiI do not generate H_2S, but still react with H_2O to form the insulating solid products of LiOH and LiI·H_2O. Combining measurements of H_2S generation with ionic conductivity therefore provides a more complete characterization of moisture stability.

$$Li_2S + 2H_2O \rightarrow H_2S\uparrow + 2LiOH \quad (2)$$

TABLE 3 | Ionic conductivity and H_2S generation data for LPSI SSE powders exposed to a −40°C dew point dry room environment as a slurry for 30 min.

Sample	Pristine σ (mS/cm)	Exposed σ (mS/cm)	Δσ w.r.t. dry LPSI (%)	H2S generation (cc/g)
Dry 75-25 LPSI powder	1.21	0.39	67.8	0.1
75-25 LPSI + Dodecane	1.21	1.04	14.0	0.0
75-25 LPSI + Anisole	1.21	0.613	49.6	0.1

$$Li_2O + H_2O \rightarrow 2LiOH \quad (3)$$

$$Li_2I + H_2O \rightarrow LiI \times H_2O \quad (4)$$

In the next experiment, the moisture stability of 75-25 LPSI was measured as a function of dew point and the data are provided in **Figure 8**. H_2S generation is not reported since the maximum value at the end of each 30 min exposure was below the 0.1 ppm detection limit of our sensor. Pristine 75-25 LPSI has an ionic conductivity of 1.21 mS/cm at room temperature when only handled inside an inert glovebox with 1 ppm H_2O (-76°C dewpoint). Exposing 75-25 LPSI powder to a dry room environment results in degradation of ionic conductivity that trends as the negative log of moisture content (**Figure 8**). This result implies that over-sizing dry room air handling equipment may not adequately address the poor moisture stability of sulfide SSEs. Designing a dry room to maintain a moisture level of less than −60°C dew point is prohibitively expensive.

Solid-state batteries will likely be manufactured using tape casting processes analogous to those used to fabricate conventional Li-ion battery electrodes. Exposure of slurries therefore better simulates the handling of sulfide SSEs in an actual manufacturing process. As a final experiment, slurries of 75-25 LPSI were prepared with either dodecane or anisole and exposed to a −40°C dew point dry room and the data are provided in **Table 3**. The solvents were also dried with 3Å molecular sieve prior to use. After exposure to a dry room environment while immersed in dodecane, the ionic conductivity of 75-25 LPSI dropped by only 14% (**Figure 8** star). On the other hand, the ionic conductivity of 75-25 LPSI dropped by 49.6% when exposed to a dry room environment while immersed in anisole. The degradation in ionic conductivity is attributed to two sources of water; namely, trace moisture in the solvent and moisture in the air. To determine what fraction of the degradation should be attributed to trace moisture in the solvent, 75-25 LPSI was soaked in dodecane or anisole while being kept inside an inert, argon-filled glovebox. This yielded a 1.7 and 16.5% drop in ionic conductivity for 75-25 LPSI soaked in dodecane and anisole, respectively. pXRD patterns of these 75-25 LPSI samples are also provided in **Supplementary Figure S2**. We conclude that a majority of the ionic conductivity degradation should be attributed to moisture from the air. The difference between samples can be explained by the fact that anisole's miscibility with water (1.6 g/L) is much higher than that of dodecane (4.91×10^{-6} g/L) (Desmurs and Ratton, 1996; ECHA, n, d). Dodecane's immiscibility with water makes it easier to dry with molecular sieve and protects the sulfide SSE from hydrolysis just like a hydrophilic polystyrene-block-polyethylene-ranbutylene-block-polystyrene (SEBS) binder was recently shown to do the same for Li_6PS_5Cl (Tan et al., 2019).

CONCLUSION

We conclude that moisture stability is best defined as a combination of H_2S gas generation and ionic conductivity measurement. Furthermore, sulfide SSEs can be handled in a dry room environment provided that the SSE composition is chosen appropriately and proper engineering controls are put in place. Sulfide SSEs will be handled in a dry room in the presence of solvents and binders and the measurement of moisture stability should seek to mimic this condition. Our results also reinforce the importance of water immiscible solvents for sulfide SSE slurries.

DATA AVAILABILITY STATEMENT

The original contributions presented in the study are included in the article/**Supplementary Material**, further inquiries can be directed to the corresponding author.

AUTHOR CONTRIBUTIONS

TY conceived the work, collected data, and wrote the manuscript. YZ and FH collected data, analyzed the results, and contributed to writing the manuscript. MC contributed to writing and reviewing the manuscript.

FUNDING

This work was funded by the Battery Materials Research Program (BMR) in the United States Department of Energy's (DOE) Office of Energy Efficiency and Renewable Energy's (EERE) Vehicle Technology Office (VTO) (DE-EE0008857).

ACKNOWLEDGMENTS

We would like to thank our colleagues for their support of our project; namely, Drs. Nicholas Pieczonka, Michael Balogh, and James Salvador.

SUPPLEMENTARY MATERIAL

The Supplementary Material for this article can be found online at: https://www.frontiersin.org/articles/10.3389/fenrg.2022.882508/full#supplementary-material

REFERENCES

Calpa, M., Rosero-Navarro, N. C., Miura, A., Jalem, R., Tateyama, Y., and Tadanaga, K. (2021). Chemical Stability of Li4PS4I Solid Electrolyte against Hydrolysis. *Appl. Mater. Today* 22, 100918. doi:10.1016/j.apmt.2020.100918

Chen, J., Wu, J., Wang, X., Zhou, A., and Yang, Z. (2021). Research Progress and Application prospect of Solid-State Electrolytes in Commercial Lithium-Ion Power Batteries. *Energ. Storage Mater.* 35, 70–87. doi:10.1016/j.ensm.2020.11.017

Chen, R., Li, Q., Yu, X., Chen, L., and Li, H. (2019). Approaching Practically Accessible Solid-State Batteries: Stability Issues Related to Solid Electrolytes and Interfaces. *Chem. Rev.* 120 (14), 6820–6877. doi:10.1021/acs.chemrev.9b00268

Desmurs, J.-R., and Ratton, S. (1996). Anisole: an Excellent Solvent. *Ind. Chem. Libr.* 8, 481–488. doi:10.1016/s0926-9614(96)80035-9

ECHA (). Dodecane Water Solubility. Available at: https://echa.europa.eu/registration-dossier/-/registered-dossier/13433/4/9 (Accessed: January 28, 2022).

Evans, C. L. (1967). The Toxicity of Hydrogen Sulphide and Other Sulphides. *Exp. Physiol.* 52 (3), 231–248. doi:10.1113/expphysiol.1967.sp001909

Hao, F., Han, F., Liang, Y., Wang, C., and Yao, Y. (2018). Architectural Design and Fabrication Approaches for Solid-State Batteries. *MRS Bull.* 43 (10), 775–781. doi:10.1557/mrs.2018.211

Hayashi, A., Muramatsu, H., Ohtomo, T., Hama, S., and Tatsumisago, M. (2014). Improved Chemical Stability and Cyclability in Li2S-P2s5-P2o5-ZnO Composite Electrolytes for All-Solid-State Rechargeable Lithium Batteries. *J. alloys Compd.* 591, 247–250. doi:10.1016/j.jallcom.2013.12.191

Hayashi, A., Muramatsu, H., Ohtomo, T., Hama, S., and Tatsumisago, M. (2013). Improvement of Chemical Stability of Li3PS4 Glass Electrolytes by Adding MxOy (M = Fe, Zn, and Bi) Nanoparticles. *J. Mater. Chem. A.* 1 (21), 6320–6326. doi:10.1039/c3ta10247e

Jain, A., Ong, S. P., Hautier, G., Chen, W., Richards, W. D., Dacek, S., et al. (2013). Commentary: The Materials Project: A Materials Genome Approach to Accelerating Materials Innovation. *APL materials* 1 (1), 011002.

Martin, S. W. (2016). "Glass and Glass-Ceramic Sulfide and Oxy-Sulfide Solid Electrolytes," in *Handbook of Solid State Batteries*, 433–501.

Muramatsu, H., Hayashi, A., Ohtomo, T., Hama, S., and Tatsumisago, M. (2011). Structural Change of Li2S-P2s5 Sulfide Solid Electrolytes in the Atmosphere. *Solid State Ionics* 182 (1), 116–119. doi:10.1016/j.ssi.2010.10.013

Ohtomo, T., Hayashi, A., Tatsumisago, M., and Kawamoto, K. (2013c). All-solid-state Batteries with Li2O-Li2S-P2s5 Glass Electrolytes Synthesized by Two-step Mechanical Milling. *J. Solid State. Electrochem.* 17 (10), 2551–2557. doi:10.1007/s10008-013-2149-5

Ohtomo, T., Hayashi, A., Tatsumisago, M., and Kawamoto, K. (2013a). Characteristics of the Li2O-Li2S-P2s5 Glasses Synthesized by the Two-step Mechanical Milling. *J. non-crystalline Sol.* 364, 57–61. doi:10.1016/j.jnoncrysol.2012.12.044

Ohtomo, T., Hayashi, A., Tatsumisago, M., and Kawamoto, K. (2013b). Glass Electrolytes with High Ion Conductivity and High Chemical Stability in the System LiI-Li2O-Li2S-P2s5. *Electrochemistry* 81 (6), 428–431. doi:10.5796/electrochemistry.81.428

Ohtomo, T., Hayashi, A., Tatsumisago, M., and Kawamoto, K. (2013d). Suppression of H2S Gas Generation from the 75Li2S·25P2S5 Glass Electrolyte by Additives. *J. Mater. Sci.* 48 (11), 4137–4142. doi:10.1007/s10853-013-7226-8

Pang, B., Gan, Y., Xia, Y., Huang, H., He, X., and Zhang, W. (2022). Regulation of the Interfaces between Argyrodite Solid Electrolytes and Lithium Metal Anode. *Front. Chem.* 10, 837978. doi:10.3389/fchem.2022.837978

Randau, S., Weber, D. A., Kötz, O., Koerver, R., Braun, P., Weber, A., et al. (2020). Benchmarking the Performance of All-Solid-State Lithium Batteries. *Nat. Energ.* 5 (3), 259–270. doi:10.1038/s41560-020-0565-1

Tan, D. H. S., Banerjee, A., Deng, Z., Wu, E. A., Nguyen, H., Doux, J.-M., et al. (2019). Enabling Thin and Flexible Solid-State Composite Electrolytes by the Scalable Solution Process. *ACS Appl. Energ. Mater.* 2 (9), 6542–6550. doi:10.1021/acsaem.9b01111

Zhang, J., Zheng, C., Li, L., Xia, Y., Huang, H., Gan, Y., et al. (2020). Lithium Batteries: Unraveling the Intra and Intercycle Interfacial Evolution of Li 6 PS 5 Cl-Based All-Solid-State Lithium Batteries (Adv. Energy Mater. 4/2020). *Adv. Energ. Mater.* 10, 2070017. doi:10.1002/aenm.202070017

Zheng, C., Wang, K., Li, L., Huang, H., Liang, C., Gan, Y., et al. (2021b). High-Performance All-Solid-State Lithium–Sulfur Batteries Enabled by Slurry-Coated Li_6PS_5Cl/S/C Composite Electrodes. *Front. Energ. Res.* 8, 606494. doi:10.3389/fenrg.2020.606494

Zheng, C., Zhang, J., Xia, Y., Huang, H., Gan, Y., Liang, C., et al. (2021a). Unprecedented Self-Healing Effect of Li 6 PS 5 Cl-Based All-Solid-State Lithium Battery. *Small* 17, 2101326. doi:10.1002/smll.202101326

Conflict of Interest: TY and MC are employed by General Motors Company. FH and YZ are employed by Optimal, Inc.

The authors declare that the research was conducted in the absence of any commercial or financial relationships that could be construed as a potential conflict of interest.

Publisher's Note: All claims expressed in this article are solely those of the authors and do not necessarily represent those of their affiliated organizations, or those of the publisher, the editors and the reviewers. Any product that may be evaluated in this article, or claim that may be made by its manufacturer, is not guaranteed or endorsed by the publisher.